TECHNICAL UNIVERSITY OF CLUJ-NAPOCA

ACTA TECHNICA NAPOCENSIS

Series: Applied Mathematics, Mechanics, and Engineering
Vol. 65, Issue Special II, September, 2022

KINEMATICS AND WORKSPACE SIMULATION OF A NEW PARALLEL ROBOT FOR SILS

Ionut ULINICI, Calin VAIDA, Bogdan GHERMAN, Tiberiu ANTAL, Paul TUCAN, Doina PISLA

Abstract: *The current paper approaches the conceptual design of a new 6 DOF parallel robot for SILS. The kinematic modelling and workspace simulation for different angular configurations of the robot platform is presented, demonstrating the best configuration that provides a wide workspace feasible for the accomplishing of the surgical task. The preliminary CAD design of the robot and the instrument platform is shown, as well as the placement of the robotic platform within a simulated operating room environment.*
Key words: *Parallel Robot, Kinematics, Workspace, SILS, modeling, simulation.*

1. INTRODUCTION

Robotics has been applied within the medical field since the end of the last millennia, when surgeons have been provided with assistive robotic systems that present increased precision, instrument motion stability necessary for human subjects [1]. In 2001 the first long range remote operated tele-surgery was performed by Dr. Marescaux, using the ZEUS robotic system [2]. Following the development of less invasive surgical procedures, the development of surgical robotics also changed. While open surgery (which implied large incisions to grant access to the surgical site) has been used for a long period of time, the need to reduce damage to healthy tissue, reduce risks to the patients (such as infection) and increase cosmesis (not leave massive scars following a surgical procedure), minimally invasive surgery or laparoscopic surgery, was born. This method uses multiple small incisions, through which the instruments are inserted (Fig. 1.C). The use of this kind of technique resulted in less damage to healthy tissue, reduced blood loss, reduced trauma, faster post-surgical recovery rates, increased cosmesis [3], etc.

Continuing from minimally invasive surgery (MIS), another technique has started to be used, namely single incision laparoscopic surgery (SILS) which seeks to reduce damage to healthy tissue even further by using a single incision between 2.5 and 3 centimeters as an entry point into the patient's body.

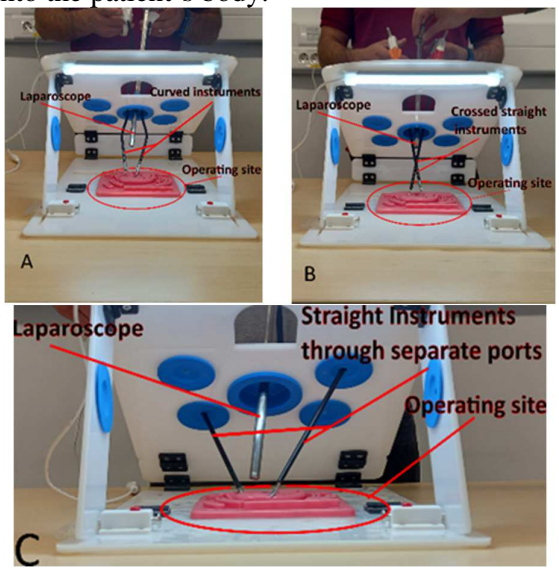

Fig.1. Instrument configurations A-SILS curved, B-SILS crossed, C-MIS

This technique implies the use of a SILS port inserted into the incision, the port usually has several valves to allow the insertion of two instruments, and a laparoscope. While at first the technique had an increased difficulty to conventional MIS, due to the crossing of instruments (Fig.1.B) and the need to use a single point of motion for both instruments and

laparoscope, this problem was approached via the development of curved (Fig.1.A) and flexible instruments [4].

Robotic SILS systems have been introduced in the surgical stage over the past few decades. The adoption of these technologies allows for more precise and collision free approaches following the workspace limitations that come with using a single incision. Furthermore, robotic systems use flexible and actuated surgical instruments that present the same if not better precision compared to conventional manual instrumentation. Advanced AR VR and sensor technologies [5-6] implemented within these systems can also provide additional data regarding the operating site and the real-time state of the patient, and surgical site [7]. Robotic SILS has proven as a feasible alternative to manual SILS, presenting the advantages of lesser post-operative pain, shorter recovery times, lesser intra-operative bleeding, and in the case of unexperienced surgeons a shorter learning curve compared to manual SILS. Although in many cases the differences between these parameters in robotic SILS and manual SILS have been classified as negligible, most studies comparing the two being limited by a small sample size [8-10]. Of the available robotic systems, the most well-known is the da Vinci Xi Surgical System. In the case of SILS it uses instruments with a semi-rigid design able to pass through a 5-lumen port made for a 25mm incision, while maintaining remote center of motion capabilities [11]. During single port robotic assisted radical prostatectomy, performed on 10 patients aged 55-77, seven were discharged on post-operative day 1 and three on day 2, there were no conversions to open surgery and no patients required pain medication on their first routine follow-up. Recently though a dedicated model called da Vinci SP, has been developed specifically for single port surgery, the devices uses a tubular arm ,which contains actuated instruments and a camera inside, which can be introduced through the incision into the patient's body, and presents its incorporated SILS port. Another device that has been used in clinical gynecological surgeries is the Senhance system. The robot system comprises three arms, each individually mounted on its own cart. Laparoscopic style handles provide haptic feedback from the cable-actuated arms, which provide 7 DOF. Senhance has been used in a 6-month study on 45 patients requiring surgery for inflammatory bowel disease, colorectal cancer, adenoma, and complicated diverticular disease, Senhance was declared to be feasible and safe. Three procedures were converted to standard laparoscopy, with postoperative complication rates reported as 35.5% [12]. Another device would be a console-based platform for laparo-endoscopic single site surgery, the Single Port Orifice Robotic Technology (SPORT) Surgical System (Titan Medical Inc.), it is composed of a workstation and robotic platform controlled by the surgeon via hand controllers, foot pedals, and a touchscreen. The workstation allows the surgeon to interact with the robotic platform, including a 3D–HD endoscopic view. The design utilizes a foldable system that can be inserted into the body cavity through a single 25 mm incision.

The reasoning behind the research presented in this paper is to obtain the geometric and workspace modelling of a 6DOF parallel robot [13-15], to demonstrate its capability of being used in SILS surgery.

The paper is further divided into 4 sections. Section 2 presents the kinematic scheme, and inverse geometric modelling of the robotic platform. Section 3, presents the preliminary CAD design of the robot, the instrument platform and workspace analysis of the robotic platform. Within this section a dimensional CAD design of the robot in a simulated operating room environment is presented. Section 4 presents the conclusions of the study in this paper.

2. A 6 DOF parallel robot for SILS

During a single incision surgical procedure, a SILS port is inserted through a 25-30 mm incision into the patient's body [16]. This port contains several access valves through which the optical device (laparoscope/laparoscopic camera) is introduced and in a conventional situation two surgical instruments (generally a grasper and scissor, scalper, electro-cauterizer, etc.) as well as additional instrumentation. As SILS uses only one access point for all

instruments, these use independent RCM's that are in close proximity to each other, at the level of the entry point into the surgical site [17]. For this purpose, the robotic system proposed in this paper uses a mobile 6 DOF platform which performs the positioning and orientation of the instruments and laparoscope with the entry valves of a SILS port. After the platform achieves the insertion into the operation site via the 6 DOF mechanism of the robot, the platform's motions are used to orient the laparoscope within the patient's body, the instruments placed on the platform are to be actuated independently from the platform to fulfill their task and to maintain the orientation of the instruments. The kinematic scheme of the robotic device is presented in figure 3.

In accordance with the kinematic scheme (Fig.3.), the 6 DOF robot is comprised of three independent kinematic chains working together, to achieve the manipulation of the platform (Fig.2.). The three kinematic chains are placed on a fixed base located at the patient's side during the operation.

The OXYZ fixed coordinate system is defined, being positioned in the vertical plane determined by the prismatic joints with free rotation C_{Ji}, i=1..3 and prismatic joints T_{Ji}, i=1..3. The coordinate system is placed on a line parallel with the translational axis of the C_{J1} and C_{J2} cylindrical joints at the bottom of their median vertical axis, which also represents the lower limit of C_{J2}'s translation, with the positive direction of the OX axis pointing back from the plane of motion of the T_{Ji} prismatic joints, the OY positive being in the direction of the C_{J3} rotation axis, and the positive Z outwards along the C_{J1} and C_{J2} rotation axes.

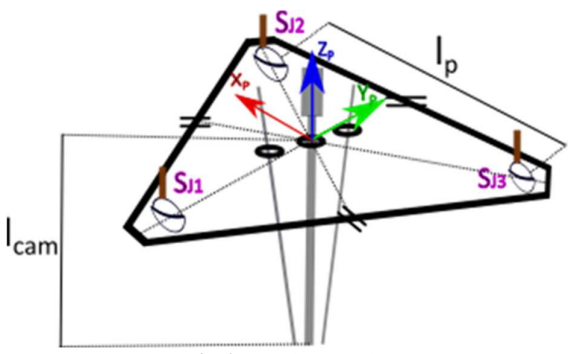

Fig.2. Platform View

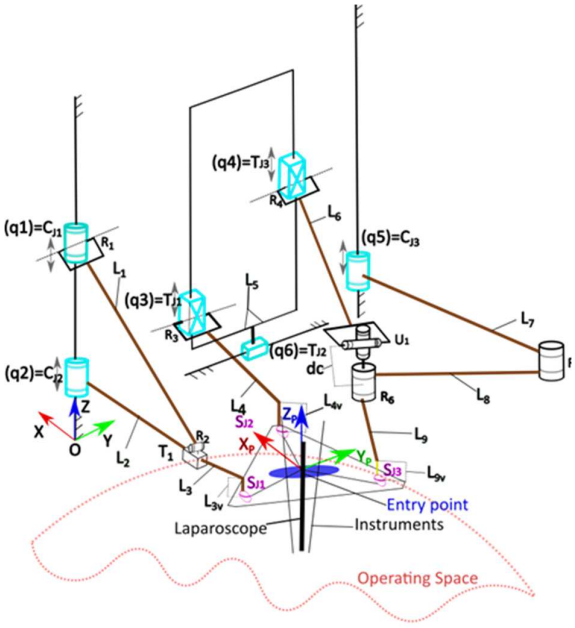

Fig.3. 6 DOF Robot Kinematic Scheme

The $OX_PY_PZ_P$ mobile coordinate system used in the definition of the mobile platform's kinematic characteristics is placed at the insertion point of the laparoscope, representing the height intersection of the equilateral triangle defined by the three center points of the spherical joints S_{Ji}, i=1…3. The three kinematic chains are as follows:

K_{Cin1} is actuated by the translation joints C_{J1} and C_{J2}, contains two passive rotation joints (R_1 and R_2), one passive translation joint T_1 and one passive spherical joint (S_{J1}), with a free motion around the axes of C_{J1} and C_{J2}.

K_{cin2} is actuated by the translation of the joint T_{J1} and contains one passive rotation joint R_3 and the passive spherical joint S_{J2}.

K_{cin3} is actuated by the translation of joint T_{J3} and C_{J3} and contains three passive rotation joints (R_3, R_4 and R_5), a passive universal joint U_1 and the passive spherical joint S_{J3}.

Additionally, K_{cin2} and K_{cin3} are connected through T_{J2} which is used when the platform (Fig.3.) needs to execute a motion along the horizontal XOY plane. Ultimately the actuated motions of the kinematic chains, through the spherical joints lead to the positioning and orientation of the instrument platform.

The kinematic modelling of the robotic device followed the approach presented in [18-20] and it should also be mentioned that the

conceptual design of this 6 DOF parallel structure, used the advantages of planar and spatial 3 DOF structures, such as 3RUU and 3RPR were taken into consideration [21-22].

2.1 The inverse geometric model

Based on the kinematic scheme (Fig.1.) and the platform scheme (Fig.2.), to obtain the solutions for the geometric model of the robotic device, the following parameters need to be introduced: l_{cam} - the length of the instruments/camera from the platform to its tip; l_p - defined as the distance between the centers of the two spherical joints ; hp – the height of the equilateral triangle determined by the three spherical joint centers; L_1 – the length of the segment between C_{J1} and the center of T_1; L_2 – the length of the segment between CJ2 and T_1; L_3 – The length of the segment from T_1 and the vertical axis of the center point of S_{J1}; L_{3v} – the distance between the center point of S_{J1} and L_3; L_4 – the segment between T_{J1} and the vertical axis of the center point of S_{J2}; L_{4v} – the distance between the center point of S_{J2} and L_4; L_5 – the fixed distance between T_{J1} and T_{J3} ; L_6 – the segment between T_{J3} and the passive universal joint U_1; L_7 – the segment between C_{J3} and passive joint R_5; L_8 – the segment between R_5 and R_6; dc – the distance between R_6 and U_1; L_9 – the segment between R6 and the vertical axis of the center point of S_{J3} and L_{9v} – the distance between the center point of S_{J3} and L_9.

Kinematically, the end effector coordinates for this system can be considered as the coordinates and orientation at the tip of the laparoscope, represented by the point $P(X_P, Y_P, Z_P)$ and angles $(\psi_P, \theta_P, \varphi_P)$.

For the inverse geometrical model, the inputs are the 6 independent coordinates of the laparoscope with respect to the fixed coordinate system. First, the generalized coordinates of the spherical joints must be calculated. These can be expressed in relation to the end effector coordinates in the mobile coordinate system pertaining to the mobile platform:

$$S_1:\begin{cases} X_{S_1}=\frac{1}{3}h_P \\ Y_{S_1}=-\frac{1}{2}l_P \\ Z_{S_1}=l_{cam} \end{cases},\ S_2:\begin{cases} X_{S_2}=-\frac{2}{3}h_P \\ Y_{S_2}=0 \\ Z_{S_2}=l_{cam} \end{cases},\quad S_3:\begin{cases} X_{S_3}=\frac{1}{3}h_P \\ Y_{S_3}=\frac{1}{2}l_P \\ Z_{S_3}=l_{cam} \end{cases} \tag{1}$$

Between the mobile and fixed coordinates of the S_i points there is the following equation:

$$S_i:\begin{bmatrix} X_{Si} \\ Y_{Si} \\ Z_{Si} \end{bmatrix}=\begin{bmatrix} X_E \\ Y_E \\ Z_E \end{bmatrix}+\begin{bmatrix} c_{11} & c_{12} & c_{13} \\ c_{21} & c_{22} & c_{23} \\ c_{31} & c_{32} & c_{33} \end{bmatrix}\cdot\begin{bmatrix} x_{Si} \\ y_{Si} \\ z_{Si} \end{bmatrix},\quad i=1..3 \tag{2}$$

Where $c_{i,j}, i, j = 1..3$ are the elements of the rotation matrix defined by the angles $(\psi_P, \theta_P, \varphi_P)$ .Using the *XYZ* convention, the terms of the rotation matrix are:

$$R:\begin{bmatrix} c_\theta c_\varphi & -c_\theta s_\varphi & s_\theta \\ s_\psi s_\theta c_\varphi + c_\psi s_\varphi & -s_\psi s_\theta s_\varphi + c_\psi c_\varphi & -s_\psi c_\theta \\ -c_\psi s_\theta c_\varphi + s_\psi s_\varphi & c_\psi s_\theta s_\varphi + s_\psi c_\varphi & c_\psi c_\varphi \end{bmatrix} \tag{3}$$

where:

$c_a : \cos(a),\ s_a : \sin(a),$ and: $\psi = \psi_P, \theta = \theta_P, \varphi = \varphi_P$

Using eq. (1-3), the coordinates for the spherical Joints S_{Ji} are:

$$\begin{cases} X_{S1} = X_p + \frac{1}{3}h_P\,c_\theta\,c_\varphi + \frac{1}{2}l_P\,c_\theta\,s_\varphi + l_{cam}\,s_\theta \\ Y_{S1} = Y_P + \frac{1}{3}h_P\left(s_\psi\,s_\theta\,c_\varphi + c_\psi\,s_\varphi\right) - \\ \quad -\frac{1}{2}l_P\left(-s_\psi\,s_\theta\,s_\varphi + c_\psi\,c_\varphi\right) - l_{cam}\,s_\psi\,c_\theta \\ Z_{S1} = Z_P + \frac{1}{3}h_P\left(-c_\psi\,s_\theta\,c_\varphi + s_\psi\,s_\varphi\right) - \\ \quad -\frac{1}{2}l_P\left(c_\psi\,s_\theta\,s_\varphi + s_\psi\,c_\varphi\right) + l_{cam}\,c_\psi\,c_\theta \end{cases} \tag{4}$$

$$\begin{cases} X_{S2} = X_p - \frac{2}{3}h_P\,c_\theta\,c_\varphi + l_{cam}\,s_\theta \\ Y_{S2} = Y_P - \frac{2}{3}h_P\left(s_\psi\,s_\theta\,c_\varphi + c_\psi\,s_\varphi\right) - l_{cam}\,s_\psi\,c_\theta \\ Z_{S2} = Z_P - \frac{2}{3}h_P\left(-c_\psi\,s_\theta\,c_\varphi + s_\psi\,s_\varphi\right) - l_{cam}\,s_\psi\,c_\theta \end{cases} \tag{5}$$

$$\begin{cases} X_{S3} = X_p + \frac{1}{3} h_P \, c_\theta \, c_\varphi - \frac{1}{2} l_P \, c_\theta \, s_\varphi + l_{cam} \, s_\theta \\ Y_{S3} = Y_P + \frac{1}{3} h_P \left(s_\psi \, s_\theta \, c_\varphi + c_\psi \, s_\varphi \right) - \\ \quad - \frac{1}{2} l_P \left(- s_\psi \, s_\theta \, s_\varphi + c_\psi \, c_\varphi \right) - l_{cam} \, s_\psi \, c_\theta \\ Z_{S3} = Z_P + \frac{1}{3} h_P \left(- c_\psi \, s_\theta \, c_\varphi + s_\psi \, s_\varphi \right) - \\ \quad - \frac{1}{2} l_P \left(c_\psi \, s_\theta \, s_\varphi + s_\psi \, c_\varphi \right) + l_{cam} \, c_\psi \, c_\theta \end{cases} \quad (6)$$

For the computation of the active joints the coordinates of joint C_{J2} must be defined, as such there are:

$$\begin{cases} X_{Cj2} = 0 \\ Y_{Cj2} = 0 \\ Z_{Cj2} = Z_{S1} + L_{3v} \end{cases} \quad (7)$$

Furthermore, there is the distance between the center of the spherical joint S_{J1} and the axis of joint C_{J2}:

$$D_{CjS} = \sqrt{X_{S1}^{\,2} + Y_{S1}^{\,2}} \quad (8)$$

From these are obtained the equations defining q_1 for joint C_{J1} and q_2 for C_{J2} from K_{cin1} with the representation of C_{J1} being dependent on q_2 and the variable distance between them, with L_{R1} and L_{R2} representing the minute displacement between the C_{J1} and center of rotation of passive joint R_1 and L_{R2} being the displacement between L_2 and the rotation center of passive joint R_2:

$$\begin{cases} q_2 = Z_{Cj2} \\ q_1 = \sqrt{L_1^{\,2} - \left(D_{CjS} - L_3 - L_{R1} + L_{R2} \right)^2} + \\ \quad + q_2 \end{cases} \quad (9)$$

For the second kinematic chain, using the coordinates for joints T_{J1} and T_{J2} used to obtain the equations of q_3 and q_4 respectively:

$$\begin{cases} X_{Tj1} = 0 \\ Y_{Tj1} = Y_{S2} \\ Z_{Tj1} = Z_{S2} + \sqrt{L_4^{\,2} - X_{S2}^{\,2}} \end{cases} \quad (10)$$

For T_{J1} and for T_{J2}:

$$\begin{cases} X_{Tj2} = 0 \\ Y_{Tj2} = Y_{S2} + \frac{1}{2} L_5 \\ Z_{Tj2} = 0 \end{cases} \quad (11)$$

Thus, there are the values for q_3 and q_4:

$$\begin{cases} q_3 = Z_{Tj1} \\ q_4 = Y_{Tj2} \end{cases} \quad (12)$$

For the third and final kinematic chain the following coordinates necessary to achieve a definition of q_5 and q_6 are obtained:

$$\begin{cases} X_{Tj3} = 0 \\ Y_{Tj3} = q_4 + \frac{L_5}{2} \\ Z_{Rp6} = Z_{S3} + L_{9v} \end{cases}$$

$$\begin{cases} X_{Rp6} = X_{S3} - \sqrt{L_9^{\,2} - (Y_{Rp6} - Y_{S3})^2} \\ Y_{Rp6} = q_4 + \frac{L_5}{2} \end{cases} \quad (13)$$

$$Z_{Tj3} = Z_{S3} + dc + \sqrt{L_6^{\,2} - X_{Rp6}^{\,2}}$$

Thus obtaining the values for:

$$\begin{cases} q_5 = Z_{Tj3} \\ q_6 = Z_{S3} + L_{9v} \end{cases} \quad (14)$$

As such the equations defining the positions of the active joints are obtained.

2.2 The inverse kinematic model

For the inverse kinematic model the input data is given by the positions, speeds and accelerations of the independent coordinates of the end-effector tip aiming to compute the positions, speeds and accelerations for the active joints. From equations 1-14, the closure equations can be obtained.

When computing the partial derivatives of the matrix A terms, one must use the initial form of the terms which depend on the independent coordinates of the end-effector, which return lengthy elements (A_{ij}, B_{54}) which will not be presented in the paper.

$$\begin{cases} f_1 = q_1 - L_{3v} - Z_{S3} \\ f_2 = q_1 - q_2 - \sqrt{\left(L_1^{\,2} - \sqrt{X_{S1}^2 - Y_{S1}^2} - L_3 \right)^2} \\ f_3 = q_3 - L_{4v} + Z_{S2} + \sqrt{\left(L_4^{\,2} - X_{S2} \right)^2} \\ f_4 = q_4 - Y_{S2} - \frac{1}{2} L_5 \end{cases} \quad (15)$$

$$\begin{cases} f_5 = q_5 - \left[Z_{S3} + dc + (\sqrt{L_6{}^2 - X_{S3}} - \right. \\ \left. - \sqrt{L_9{}^2 - \left(q_4 + \frac{1}{2} L_5 - Y_{S3} \right)^2} \right]^2 \\ f_6 = q_6 - L_{9v} - Z_{S3} \end{cases} \quad (16)$$

Based on the closure equations (15-16), the two Jacobi matrices can be computed. The general form of the two matrices, is:

$$A_{6x6} = \begin{pmatrix} \frac{\partial f_1}{\partial X_E} & \cdots & \frac{\partial f_1}{\partial \varphi} \\ \mathrm{M} & \mathrm{M} & \mathrm{M} \\ \frac{\partial f_6}{\partial X_E} & \cdots & \frac{\partial f_6}{\partial \varphi} \end{pmatrix} \quad (17)$$

$$B_{6x6} = \begin{pmatrix} \frac{\partial f_1}{\partial q_1} & \cdots & \frac{\partial f_1}{\partial q_6} \\ \mathrm{M} & \mathrm{M} & \mathrm{M} \\ \frac{\partial f_6}{\partial q_1} & \cdots & \frac{\partial f_6}{\partial q_6} \end{pmatrix} \quad (18)$$

$$A = \begin{pmatrix} 0 & 0 & -1 & A_{14} & A_{15} & A_{16} \\ A_{21} & A_{22} & 0 & A_{24} & A_{25} & A_{26} \\ A_{31} & 0 & -1 & A_{34} & A_{35} & A_{36} \\ 0 & -1 & 0 & A_{44} & A_{45} & A_{46} \\ A_{51} & A_{52} & 0 & A_{54} & A_{55} & A_{56} \\ 0 & 0 & -1 & A_{64} & A_{65} & A_{66} \end{pmatrix} \quad (19)$$

Based on the form of the implicit functions, however, matrix B has a very simple form:

$$B = \begin{pmatrix} 0 & 1 & 0 & 0 & 0 & 0 \\ 1 & -1 & 0 & 0 & 0 & 0 \\ 0 & 0 & 1 & 0 & 0 & 0 \\ 0 & 0 & 0 & 1 & 0 & 0 \\ 0 & 0 & 0 & B_{54} & 1 & 0 \\ 0 & 0 & 0 & 0 & 0 & 1 \end{pmatrix} \quad (20)$$

The following notations are introduced, representing the velocity vectors for the independent coordinates on the end-effector and respectively the active joints:

$$\dot{X} = \left[\dot{X_E}, \dot{Y}_E, \dot{Z}_E, \dot{\psi}, \dot{\theta}, \dot{\varphi} \right]^T$$
$$\dot{q} = [\dot{q}_1, \dot{q}_2, \dot{q}_3, \dot{q}_4, \dot{q}_5, \dot{q}_6]^T \quad (21)$$

Between these two vectors the following equation can be written as shown by Merlet [13]:

$$A \cdot \dot{X} + B \cdot \dot{q} = 0 \quad (22)$$

In eq. 21 the unknown is $\dot{q}$ which can be computed using the following matrix relation:

$$\dot{q} = -B^{-1} \cdot A \cdot \dot{X} \quad (23)$$

By deriving with respect to time eq. 19 results:

$$A \cdot \ddot{X} + \dot{A} \cdot \dot{X} + B \cdot \ddot{q} + \dot{B} \cdot \dot{q} = 0 \quad (24)$$

Where, $\dot{A}$and $\dot{B}$are the time derivatives of the Jacobi matrices A and B [13]. Introducing the vectors that define the accelerations of the independent coordinates of the end-effector, respectively the active joints:

$$\ddot{X} = \left[\ddot{X_E}, \ddot{Y}_E, \ddot{Z}_E, \ddot{\psi}, \ddot{\theta}, \ddot{\varphi} \right]^T$$
$$\ddot{q} = [\ddot{q}_1, \ddot{q}_2, \ddot{q}_3, \ddot{q}_4, \ddot{q}_5, \ddot{q}_6]^T \quad (25)$$

The equations for the acceleration of the active joints are computed with the following matrix equation:

$$\ddot{q} = -B^{-1} \cdot \left(\dot{A} \cdot \dot{X} + A \cdot \ddot{X} + \dot{B} \cdot \dot{q} \right) \quad (26)$$

3. Preliminary Robot Design

A preliminary design of the robotic system is shown (Fig.5.) and integrated within a CAD simulated operating room environment. The system is presented comprised of the robotic platform, instrument orientation mechanism, respecting the medical protocol and characteristics described in [13] done using the Siemens NX CAD software, and it serves for the study of its component size and size of the orientation mechanism (Fig.4.) with regards to the operating room characteristics (Fig.13).

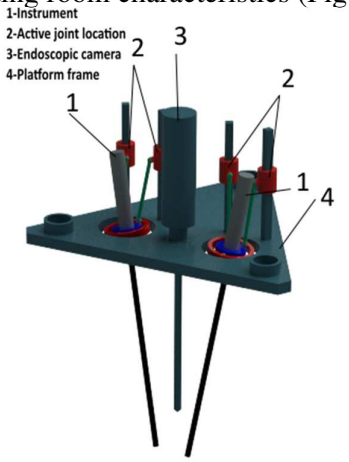

Fig.4. The Instrument Platform

For this purpose the following dimensional values were used :

$l_P = 300\,mm; l_{cam} = 300\,mm; L_1 = 550\,mm; L_2 = 300\,mm;$
$L_3 = 140\,mm L_{3v} = 70\,mm; L_4 = 420\,mm; L_{4v} = 50\,mm;$
$L_5 = 280\,mm L_6 = 465\,mm; L_7 = 350\,mm; L_8 = 390\,mm;$
$L_9 = 270\,mm L_{9v} = 120\,mm; dc = 140\,mm; L_{Rob} = 800\,mm;$
$l_{Rob} = 250\,mm; h_{Rob} = 920\,mm$

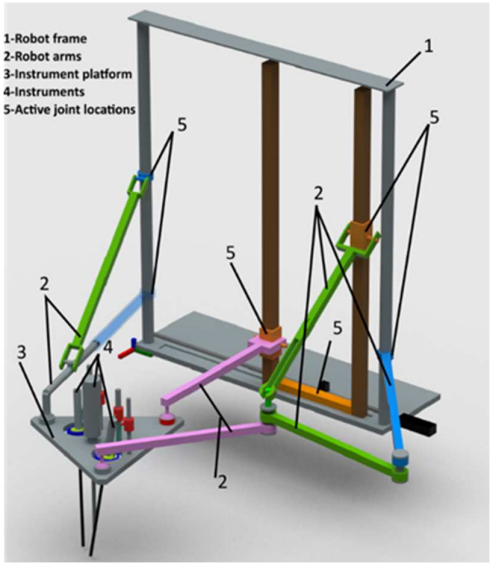

Fig.5. The Robotic System

For the workspace analysis the inverse geometrical model was used with regards to the end effector for different configurations [23]. The graphical representations were extracted from the MathWorks MATLAB software.

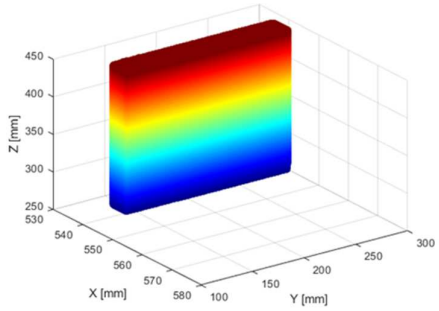

Fig.6. Workspace for $\psi = \theta = \varphi = 0^o$

Following the medical task, the only angles that should be involved in motion are the $\psi;\theta$ angles denoting rotation around the X and Y axis, while the φ angle is the one that enables the rotation of the laparoscope around its own axis. Workspace computation (Fig.6-7.) showed that the φ angle is only capable of reaching values between 0 and 14 degrees, while this shows a very limited freedom of motion, it is not one that should impact the platform's capability of fulfilling its medical task (Fig.8-12).

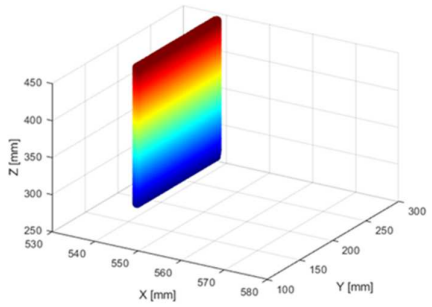

Fig.7. Workspace for $\psi = 0^o; \theta = 0^o; \varphi = 14^o$

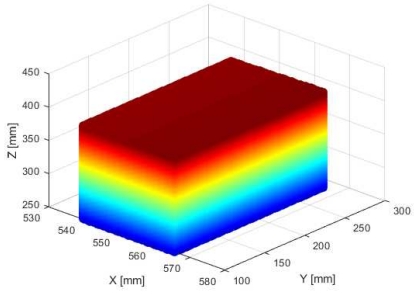

Fig.8. Workspace for $\psi = 45^o; \theta = 45^o; \varphi = 14^o$

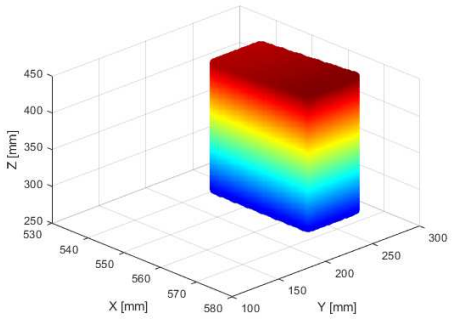

Fig.9. Workspace for $\psi = -45^o; \theta = 45^o; \varphi = 14^o$

It was observed that the ψ angle can independently reach values between -53° and 155° while θ angle can reach values between 0 and 120 degrees. The workspace graphs in figure 6-9 shows that at angular value of interest for the surgical task, the workspace is sufficient. At the same time, it was concluded that having the platform be operated while it is at an inclined angle and not parallel with the horizontal plane leads to greater workspace envelopes. Unfortunately, the angle φ cannot reach a value greater than 14° as this leads to a singularity in created by the robot arms positioning.

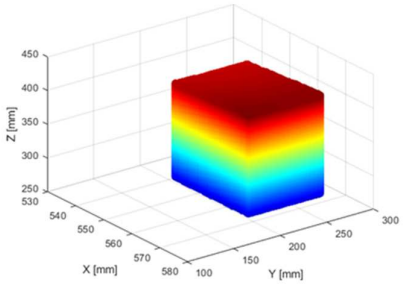

Fig.10. Workspace for $\psi = -45^o; \theta = 45^o; \varphi = 0^o$

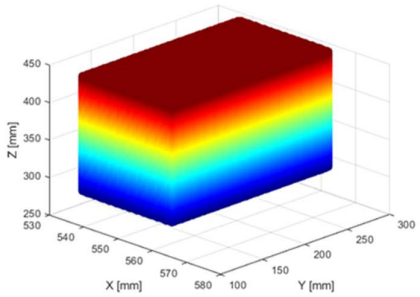

Fig.11. Workspace for $\psi = 15^o; \theta = 15^o; \varphi = 14^o$

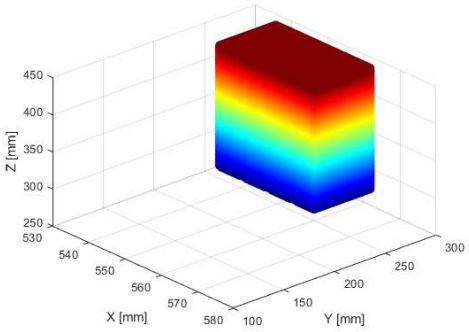

Fig.12. Workspace for $\psi = 15^o; \theta = 15^o; \varphi = 14^o$

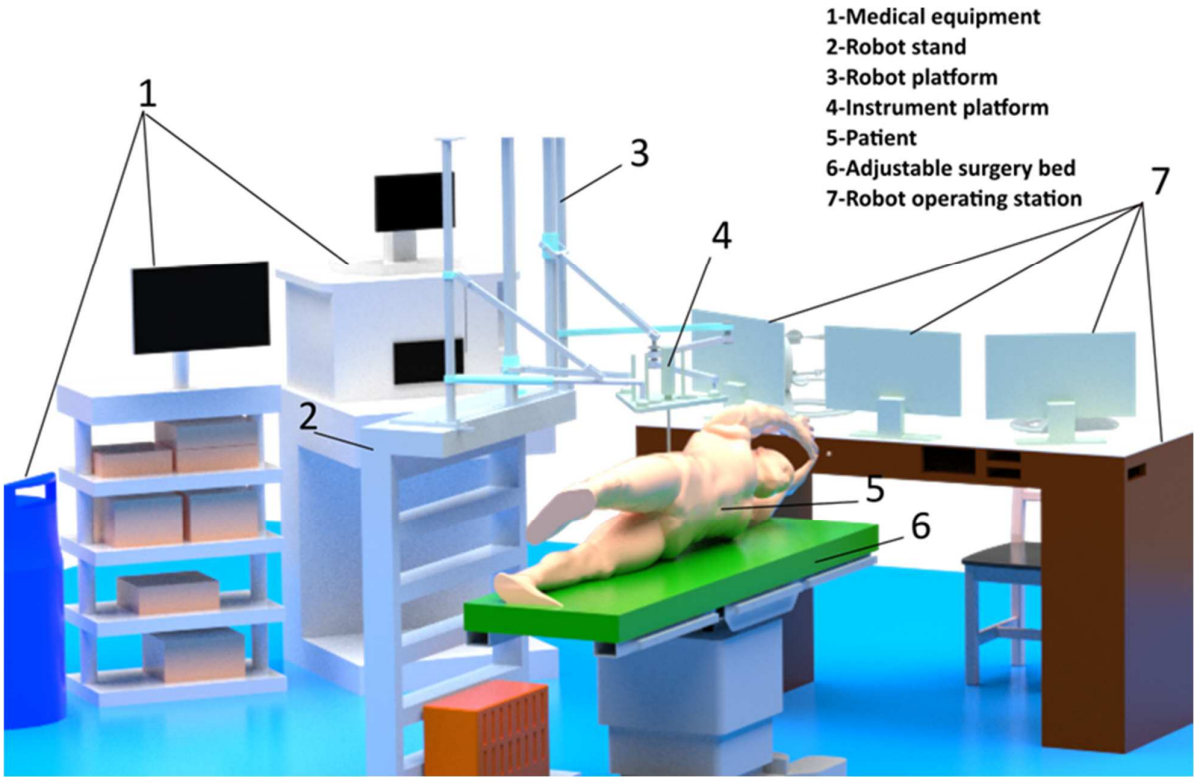

Fig.13. The Robotic device in a simulated operating room

4. Conclusions

In this paper, the inverse geometric modelling for a 6DOF robotic platform designed for instrument and laparoscope alignment and insertion within the operative space for a SILS procedure was solved. The workspace

capabilities of the robotic device were assessed, revealing a viable configuration of the end effector which can accomplish the SILS oriented task. The simplified CAD model of the robot and the end effector (instrument platform was also presented), as well as the robotic platform placed in a virtual OR environment for reference. Future work implies motion simulations of the robotic platform as well as CAD simulations of the robot assembly with respect to workspace capabilities and the geometric model, following the parameters dictated by the limitations of the surgical task the device aims to accomplish.

5. Acknowledgement

This work was supported by a grant of the Ministry of Research, Innovation and Digitization, CNCS/CCCDI – UEFISCDI, project number PCE171/2021 – Challenge within PNCDI III and by a grant of the European Social Fund through the Operational Programme for Human Capital POCU/380/6/13/123927, contract number 56437/24.07.2019.

6. REFERENCES

[1] Berceanu, C., et.al., *About an experimental approach used to determine the kinematics of the human,* Journal of Solid State Phenomena, Robotics and Automat Syst, 166-167, pp.45-50, 2010.

[2] George EI, Brand TC, LaPorta A, Marescaux J, Satava RM. *Origins of Robotic Surgery: From Skepticism to Standard of Care."JSLS*. 2018;.

[3] A. Darzi and Y. Munz, *The Impact of Minimally Invasive Surgical Techniques*, Annual Review of Medicine, vol. 55, pp. 223–237, Feb. 2004.

[4] Greaves N, Nicholson J. *Single incision laparoscopic surgery in general surgery: a review.* Ann R Coll Surg Engl. 2011;.

[5] Tarnita, D., Geonea, I.,Petcu, A., Tarnita, D.N., N*umerical Simulations and Experimental Human Gait Analysis Using Wearable Sensors*, Mechanisms and Machine Science, 48, pp. 289-304, 2018.

[6] Tarnita D., Boborelu, C., Popa, D., Rusu, L., *The three-dimensional modeling of the complex virtual human elbow joint*, Romanian Journal of Morphology and Embryology, 51(3), pp. 489-495, 2010

[7] Ho C, Tsakonas E, Tran K, et al. *Robot-Assisted Surgery Compared with Open Surgery and Laparoscopic Surgery: Clinical Effectiveness and Economic Analyses.* 2011.

[8] Ding DC, Hong MK, Chu TY, Chang YH, Liu HW. *Robotic single-site supracervical hysterectomy with manual morcellation: Preliminary experience. World J Clin Cases*. 2017;5(5):172-177.

[9] Moukarzel LA, Sinno AK, Fader AN, Tanner EJ. *Comparing Single-Site and Multiport Robotic Hysterectomy with Sentinel Lymph Node Mapping for Endometrial Cancer: Surgical Outcomes and Cost Analysis.* J Minim Invasive Gynecol. 2017 Sep-Oct;24(6):977-983.

[10] Maurice MJ, Ramirez D, Kaouk JH. *Robotic Laparoendoscopic Single-site Retroperitioneal Renal Surgery: Initial Investigation of a Purpose-built Single-port Surgical System.* Eur Urol. 2017 Apr;71(4):643-647.

[11] Armijo PR, Pagkratis S, Boilesen E, Tanner T, Oleynikov D *Growth in robotic-assisted procedures is from conversion of laparoscopic procedures and not from open surgeons' conversion: a study of trends and costs.* Surg. Endosc. (2017)

[12] Spinelli, A., David, G., Gidaro, S., Carvello, M., Sacchi, M., Montorsi, M. and Montroni, I. (2018), *First experience in colorectal surgery with a new robotic platform with haptic feedback.* Colorectal Dis, 20: 228-235.

[13] Ulinici.I, Crisan N., Vaida C., Andras I, Pisla D., *Analysis and Preliminary Design of a New Parallel Robot for SILS,* IEEE International Conference on Automation, Quality and Testing, Robotics (AQTR), 19-21.05 2022

[14] Tarnita, D., Marghitu, D., *Nonlinear dynamics of normal and osteoarthritic human knee,* Proceedings of the Romanian Academy, pp. 353-360, 2017.

[15]Tarnita, D., Georgescu, M., Tarnita, D.N., *Applications of Nonlinear Dynamics to Human knee movement on Plane & Inclined*

Treadmill, New Trends in Medical and Service Robots, Vol 39, 59-73, 2016, Springer.

[16] Tarnita, D., Pisla, D., Geonea, I., Vaida, C., I. Tarnita D.N, *Static and Dynamic Analysis of Osteoarthritic and Orthotic Human Knee*, J Bionic Eng, 16(3), pp.514-525, 2019.

[17] Vaida, C., Andras, I., Birlescu, I., Crisan, N., Plitea, N., Pisla, D., *Preliminary control design of a Single-Incision Laparoscopic Surgery Robotic System*, 25th International Conference on System Theory, Control and Computing (ICSTCC), IEEE, pp. 384-289, 2021

[18] Pisla, D., Andras, I., Vaida, C., Crisan, N., Ulinici, I., Birlescu, I., Plitea, N. *New Approach to Hybrid Robotic System Application in Single Incision Laparoscopic Surgery*, Acta Tehnica Napocensis, Vol. 64(3), pp. 369-378, 2021

[19] Pisla, D., Plitea, N., Videan, A., Prodan, B., Gherman, B. Lese, D.*: Kinematics and design of two variants of a reconfigurable parallel robot*, ASME/IFToMM International Conference on Reconfigurable Mechanisms and Robots, pp. 624-631, 2009

[20] Pisla, D., Plitea, N., Gherman, B., Vaida, C., Pisla, A., Suciu, M., *Kinematics and design of a 5-DOF parallel robot used in minimally invasive surgery*, Advances in robot kinematics: Motion in man and machine, pp. 99-106, 2010

[21] Husty, M., Birlescu, I., Tucan, P., Vaida, C., Pisla, D.:*An algebraic parameterization approach for parallel robots analysis,* Mechanism and Machine Theory, 140, pp. 245-257, 2019

[22] Nedezki, C.M., Julean, D., Kerekes, G., (2009), *Study of the workspace for parallel manipulator 3RUU*, Annals of DAAAM for 2009 & Proceedings of 20th DAAAM International Symp, ISBN 978-3-901509-70-4, ISSN 1726-9679, pag. 1445-1446.

[23] Nedezki, C.M., *The maximal workspace with constant orientation of the 3DOF RPR parallel manipulator,* 3rd International Conference AVANCED ENGINEERING IN MECHANICAL SYSTEMS 2013, ISSN 1221-5872, Cluj-Napoca, Vol 56, Issue IV, November 2013, pp. 725-728.

,

Simularea cinematică și spațiul de lucru al unui nou sistem robotic paralel pentru SILS

Rezumat: Lucrarea actuală abordează proiectarea conceptuală a unui nou robot paralel de 6 DOF pentru SILS. Este prezentată modelarea cinematică și simularea spațiului de lucru pentru diferite configurații unghiulare ale platformei robotului, demonstrând cea mai bună configurație care oferă un spațiu larg de lucru fezabil pentru realizarea operațiunii chirurgicale. sarcină. Este prezentat proiectul CAD preliminar al robotului și al platformei de instrumente, precum și amplasarea platformei robotizate într-un mediu simulat de sală de operație.

Ionut ULINICI, PhD Student, Technical University of Cluj-Napoca, CESTERIonut.Ulinici@omt.utcluj.ro, Memorandumului 28, RO-400114 Cluj-Napoca, Romania

Calin VAIDA, Professor Dr. Eng., Technical University of Cluj-Napoca, CESTER, Calin.Vaida@mep.utcluj.ro, Memorandumului 28, RO-400114 Cluj-Napoca, Romania

Bogdan GHERMAN, Associate Professor Dr. Eng., Technical University of Cluj-Napoca, CESTER, Bogdan.Gherman@mep.utcluj.ro, Memorandumului 28, RO-400114 Cluj-Napoca, Romania.

Tiberiu ANTAL, Professor Dr. Eng., Technical University of Cluj-Napoca, CESTER antaljr@bavaria.utcluj.ro, Memorandumului 28, RO-400114 Cluj-Napoca, Romania

Paul TUCAN, Lecturer Dr. Eng., Technical University of Cluj-Napoca, CESTER, Paul.Tucan@mep.utcluj.ro, Memorandumului 28, RO-400114 Cluj-Napoca, Romania.

Doina PISLA, Professor Dr. Eng., Researcher, Technical University of Cluj-Napoca, CESTER-Research Center for Industrial Robots Simulation and Testing, Doina.Pisla@mep.utcluj.ro, Memorandumului 28, RO-400114 Cluj-Napoca, Romania